Optimization of plasmonic nanostructure for nanoparticle trapping

Jingzhi Wu and Xiaosong Gan*

Centre for Micro-Photonics, Faculty of Engineering and Industrial Sciences, Swinburne University of Technology, PO Box 218, Hawthorn, VIC-3122, Australia

**xgan@swin.edu.au*

Abstract: We present a detailed analysis of nanoparticle trapping using plasmonic nanostructures, which predicts an improvement of two orders of magnitude in trapping force obtained by optimizing the plasmon resonance of the nanostructures. As the result, a total of four orders of magnitude enhancement in trapping force can be achieved comparing to the case without the nanostructures. In addition, it is illustrated that tuning the resonance wavelength is achievable by varying the diameter and/or the height of the nanorods.

OCIS codes: (350.4855) Optical tweezers or optical manipulation; (240.6680) Surface plasmons; (310.6628) Subwavelength structures, nanostructures.

References and links

1. M. L. Juan, M. Righini, and R. Quidant, "Plasmon nano-optical tweezers," Nat. Photonics **5**(6), 349–356 (2011).
2. J. R. Moffitt, Y. R. Chemla, S. B. Smith, and C. Bustamante, "Recent advances in optical tweezers," Annu. Rev. Biochem. **77**(1), 205–228 (2008).
3. B. J. Roxworthy, K. D. Ko, A. Kumar, K. H. Fung, E. K. C. Chow, G. L. Liu, N. X. Fang, and K. C. Toussaint, Jr., "Application of plasmonic bowtie nanoantenna arrays for optical trapping, stacking, and sorting," Nano Lett. **12**(2), 796–801 (2012).
4. X. Gao and X. Gan, "Modulation of evanescent focus by localized surface plasmons waveguide," Opt. Express **17**(25), 22726–22734 (2009).
5. X. Miao and L. Y. Lin, "Trapping and manipulation of biological particles through a plasmonic platform," IEEE J. Sel. Top. Quantum Electron. **13**(6), 1655–1662 (2007).
6. X. Miao, B. K. Wilson, S. H. Pun, and L. Y. Lin, "Optical manipulation of micron/submicron sized particles and biomolecules through plasmonics," Opt. Express **16**(18), 13517–13525 (2008).
7. B. Päivänranta, H. Merbold, R. Giannini, L. Büchi, S. Gorelick, C. David, J. F. Löffler, T. Feurer, and Y. Ekinci, "High aspect ratio plasmonic nanostructures for sensing applications," ACS Nano **5**(8), 6374–6382 (2011).
8. M. Bora, B. J. Fasenfest, E. M. Behymer, A. S. P. Chang, H. T. Nguyen, J. A. Britten, C. C. Larson, J. W. Chan, R. R. Miles, and T. C. Bond, "Plasmon resonant cavities in vertical nanowire arrays," Nano Lett. **10**(8), 2832–2837 (2010).
9. A. V. Kabashin, P. Evans, S. Pastkovsky, W. Hendren, G. A. Wurtz, R. Atkinson, R. Pollard, V. A. Podolskiy, and A. V. Zayats, "Plasmonic nanorod metamaterials for biosensing," Nat. Mater. **8**(11), 867–871 (2009).
10. J. Wu and X. Gan, "Three dimensional nanoparticle trapping enhanced by surface plasmon resonance," Opt. Express **18**(26), 27619–27626 (2010).
11. A. N. Grigorenko, N. W. Roberts, M. R. Dickinson, and Y. Zhang, "Nanometric optical tweezers based on nanostructured substrates," Nat. Photonics **2**(6), 365–370 (2008).
12. W. Zhang, L. Huang, C. Santschi, and O. J. F. Martin, "Trapping and sensing 10 nm metal nanoparticles using plasmonic dipole antennas," Nano Lett. **10**(3), 1006–1011 (2010).
13. Y. Pang and R. Gordon, "Optical trapping of 12 nm dielectric spheres using double-nanoholes in a gold film," Nano Lett. **11**(9), 3763–3767 (2011).
14. M. L. Juan, R. Gordon, Y. Pang, F. Eftekhari, and R. Quidant, "Self-induced back-action optical trapping of dielectric nanoparticles," Nat. Phys. **5**(12), 915–919 (2009).
15. C. Chen, M. L. Juan, Y. Li, G. Maes, G. Borghs, P. Van Dorpe, and R. Quidant, "Enhanced optical trapping and arrangement of nano-objects in a plasmonic nanocavity," Nano Lett. **12**(1), 125–132 (2012).
16. A. E. Cetin, A. A. Yanik, C. Yilmaz, S. Somu, A. Busnaina, and H. Altug, "Monopole antenna arrays for optical trapping, spectroscopy, and sensing," Appl. Phys. Lett. **98**(11), 111110 (2011).
17. K. Wang, E. Schonbrun, P. Steinvurzel, and K. B. Crozier, "Trapping and rotating nanoparticles using a plasmonic nano-tweezer with an integrated heat sink," Nat Commun. **2**, 469 (2011).
18. D. Lapotko, "Optical excitation and detection of vapor bubbles around plasmonic nanoparticles," Opt. Express **17**(4), 2538–2556 (2009).
19. P. V. Ruijgrok, N. R. Verhart, P. Zijlstra, A. L. Tchebotareva, and M. Orrit, "Brownian fluctuations and heating of an optically aligned gold nanorod," Phys. Rev. Lett. **107**(3), 037401 (2011).

#164468 - $15.00 USD Received 9 Mar 2012; revised 28 Apr 2012; accepted 5 Jun 2012; published 19 Jun 2012

20. R. T. Schermer, C. C. Olson, J. P. Coleman, and F. Bucholtz, "Laser-induced thermophoresis of individual particles in a viscous liquid," Opt. Express **19**(11), 10571–10586 (2011).
21. X. Miao, B. K. Wilson, and L. Y. Lin, "Localized surface plasmon assisted microfluidic mixing," Appl. Phys. Lett. **92**(12), 124108 (2008).
22. H. Ditlbacher, A. Hohenau, D. Wagner, U. Kreibig, M. Rogers, F. Hofer, F. R. Aussenegg, and J. R. Krenn, "Silver nanowires as surface plasmon resonators," Phys. Rev. Lett. **95**(25), 257403 (2005).
23. J. Dorfmüller, R. Vogelgesang, W. Khunsin, C. Rockstuhl, C. Etrich, and K. Kern, "Plasmonic nanowire antennas: experiment, simulation, and theory," Nano Lett. **10**(9), 3596–3603 (2010).
24. P. B. Johnson and R. W. Christy, "Optical constants of the noble metals," Phys. Rev. B **6**(12), 4370–4379 (1972).
25. "FDTD Solutions," Lumerical Solutions Inc., *www.lumerical.com*.
26. H. Xu and M. Käll, "Surface-plasmon-enhanced optical forces in silver nanoaggregates," Phys. Rev. Lett. **89**(24), 246802 (2002).
27. H.-R. Jiang, H. Wada, N. Yoshinaga, and M. Sano, "Manipulation of colloids by a nonequilibrium depletion force in a temperature gradient," Phys. Rev. Lett. **102**(20), 208301 (2009).
28. M. Braibanti, D. Vigolo, and R. Piazza, "Does thermophoretic mobility depend on particle size?" Phys. Rev. Lett. **100**(10), 108303 (2008).
29. R. Piazza and A. Parola, "Thermophoresis in colloidal suspensions," J. Phys. Condens. Matter **20**(15), 153102 (2008).
30. S. Duhr and D. Braun, "Why molecules move along a temperature gradient," Proc. Natl. Acad. Sci. U.S.A. **103**(52), 19678–19682 (2006).
31. G. Baffou, R. Quidant, and C. Girard, "Heat generation in plasmonic nanostructures: Influence of morphology," Appl. Phys. Lett. **94**(15), 153109 (2009).
32. C. L. G. Alzar, M. A. G. Martinez, and P. Nussenzveig, "Classical analog of electromagnetically induced transparency," Am. J. Phys. **70**(1), 37–41 (2002).
33. S. Buzzi, M. Galli, M. Agio, and J. F. Loffler, "Silver high-aspect-ratio micro- and nanoimprinting for optical applications," Appl. Phys. Lett. **94**(22), 223115 (2009).

1. Introduction

Accurate three-dimensional (3D) manipulation of nanoparticles is a highly desirable technique for a range of applications such as single molecule spectroscopy, colloidal dynamics, particle assembly, and lab-on-a-chip technology [1–3]. However, trapping nanoparticles is challenging because the magnitude of optical trapping force decreases with the cube of the diameter of the nanoparticles, and the Brownian motion becomes increasingly affecting the trapping performance. For nanoparticle of size significantly smaller than the optical wavelength, the optical trapping force can be approximated as the linearly proportion to the gradient of electromagnetic (EM) field [1–3]. Therefore in order to improve the field gradient, one can either increase the strength or the confinement of the EM field. Inducing surface plasmon resonance in metallic nanostructures is a well-known technique that produces strongly enhanced and spatially confined EM field [4–9] and therefore attracts wide attention in producing plasmon-based nano-optical tweezers for nanoparticle trapping [1, 10]. For example, plasmonic antennas [1, 11, 12] and nanoholes in metallic thin film [13–15] have been demonstrated for trapping metallic and dielectric nanospheres. Periodic arrays of gold nanopillars on a metal film [7, 16, 17] have been presented for sensing applications. It is worth to be mentioned that under the laser excitation at wavelength close to the plasmon resonance wavelength, plasmonic nanostructures efficiently couple to the incident optical field and generate considerable amount of heat [1, 18, 19]. The thermally induced forces can strongly affect motions of nanoparticles and should be taken into consideration when designing efficient nano-tweezers [20, 21].

Plasmonic nanorods or nanowires are interesting for the design of optical resonators [22, 23]. It has been demonstrated previously that strong EM field enhancement and confinement in the plasmonic nano-waveguides structure provides up to two orders of magnitude stronger optical forces for trapping nanoparticles comparing with the optical trapping without the nanostructure [10]. In this work, the effects of structure parameters on plasmon resonance are studied in detail in order to further improve the trapping force of nanoparticles.

2. Trapping scheme and plasmonic nanostructure layout

The nanoparticle trapping approach is based on a plasmonic nanostructure comprising of two vertically aligned silver nanorods suspended in water (refractive index n_m = 1.33), as shown

#164468 - $15.00 USD Received 9 Mar 2012; revised 28 Apr 2012; accepted 5 Jun 2012; published 19 Jun 2012

in Fig. 1. The geometrical parameters of the nanostructure are the diameter d and height h of the nanorods, and the separation s between them. Plasmonic absorption and field distributions of the plasmonic nanostructures are calculated using a commercial Finite Difference Time Domain (FDTD) solver (Lumerical Inc, with material data for silver reported in Ref [24], mesh size 1 nm x 1 nm x 1 nm) [25]. The electric field **E**, magnetic field **H** and wavevector **k** of the excitation light, oriented along the x, y and z directions, are illustrated in Fig. 1. The excitation light is x-polarized plane wave and propagates from the substrate. For electric field calculations throughout the paper, the amplitude of the incident illumination is set as |E| = 1 V m^{-1}.

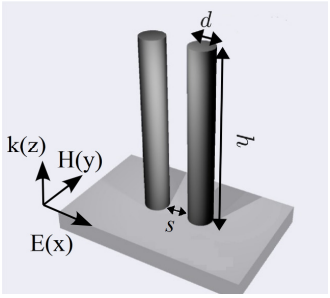

Fig. 1. Schematic diagram of the nanostructure of two silver nanorods with height h, diameter d and separation s. Incident field is x-polarized and propagates in the z direction from the substrate (refractive index 1.78) into water (refractive index n_m = 1.33). The origin of the coordinate system is at the center of the gap on the interface.

While dielectric nanoparticles are of size significantly smaller than optical wavelength, the electromagnetic trapping force is proportional to the gradient of the localized field, $F = -\frac{n_m}{2}\alpha\nabla E^2$, here α is the polarizability of the nanoparticle [10, 14, 26]. Due to the fact that the nanoparticle is small and of a refractive index of 1.5, which close to that of the surrounding medium (water, n_w = 1.33), the disturbance in the EM field caused by the presence of the nanoparticle is negligible. It has been shown that the gradient force agrees well with rigorous force calculations using Maxwell stress tensor method for nanoparticles more than 20 nm away from plasmonic nanostructures [14]. The scattering force on a 20 nm nanoparticle is about three orders magnitude smaller than the gradient force. While the nanoparticle is in the immediate vicinity of the nanostructure (e.g. <10 nm), the trapping force calculated with the perturbative method using gradient of the field is slightly smaller than that obtained with the rigorous method using the Maxwell stress tensor [14].

For low concentration of nanoparticles, the net thermal force **f** [27–30] acting on the particle by the solvent due to the present of the temperature gradient can be approximated as proportional to the temperature gradient ∇T [29], $\mathbf{f} = -S_T\nabla T/\beta$, where S_T is the Soret coefficient, $\beta = 1/k_BT$, k_B is the Boltzmann constant, T is the temperature [10]. The temperature increase around the plasmonic nanostructure can be obtained by $\Delta T(\mathbf{r}) = \frac{1}{4\pi K_m}\left(\int_V \frac{q}{r_1}dV - \frac{K_s - K_m}{K_s + K_m}\int_V \frac{q}{r_2}dV\right)$, where q is the heat generation density which is determined by energy absorption of the nanostructure [10], r_1, r_2 are the distance from the heat source element dV in the nanostructure (with volume V) and its image heat source in the substrate, to a position **r**. K_m, K_s are the thermal conductivity of the surrounding medium and the substrate respectively (K_m = 0.6 W K^{-1} m^{-1} and K_s = 1.1 W K^{-1} m^{-1} is assumed for our simulation) [10, 31].

We start by considering the optical response of the nanostructure with two silver nanorods having diameter d of 70 nm, height h of 820 nm, and separation s of 100 nm. Fig. 2(a) shows the absorption spectrum of the nanostructure. Two strong absorption peaks at wavelengths of

#164468 - $15.00 USD Received 9 Mar 2012; revised 28 Apr 2012; accepted 5 Jun 2012; published 19 Jun 2012

430 nm and 455 nm can be observed, which arise from localized surface plasmon resonance. This is because that the light polarization direction is normal to the long axis of the nanorods, only transverse plasmon modes in the plasmonic nanorods can be excited efficiently. As a result of the finite length of the nanorods, standing plasmon wave can be formed along the long axis of the nanorods [23].

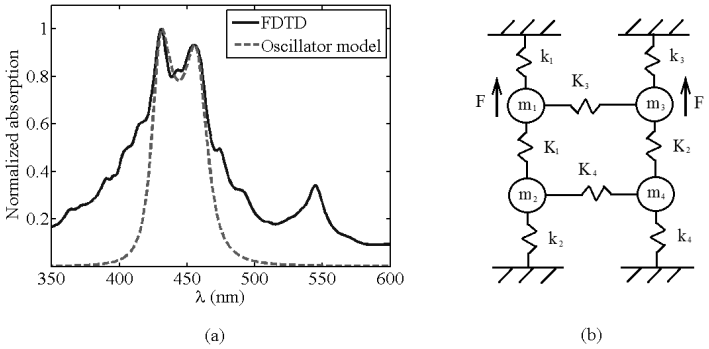

Fig. 2. (a) Absorption spectrum of the nanostructure with separation *s* of 100 nm, diameter *d* of 70 nm and height *h* of 820 nm. (b) An oscillator model for the optical response of the nanostructure.

The absorption spectrum can be explained by using a simple oscillator model [32] as shown in Fig. 2(b). Each nanorod is modeled by two harmonic oscillators (m_1, m_2) and (m_3, m_4), that are all attached to walls by springs of spring constants k_1, k_2, k_3 and k_4. The four oscillators are also interconnected with springs of spring constants K_1, K_2, K_3 and K_4. Harmonic forces $\mathbf{F} = F\exp(-i\omega_S t)$ are applied to oscillators m_1 and m_3. For simplicity, we choose $m_1 = m_2 = m_3 = m_4 = 1$, $k_1 = k_2 = k_3 = k_4 = k$, $K_1 = K_2 = K$, and $\Omega^2 = K/m$. Also using $\Omega_c^2 = K_3/m$, $\Omega_{c2}^2 = K_4/m$ for the coupling between the two nanorods, we can derive the motion equations of oscillators m_1, m_2, m_3, and m_4 as a function of displacements x_1, x_2, x_3 and x_4, from their respective equilibrium positions as,

$$\begin{aligned}
&x_1'' + \gamma_1 x_1' + \omega_1^2 x_1 - \Omega^2 x_2 - \Omega_c^2 x_3 = \frac{F}{m}\exp(-i\omega_S t),\\
&x_2'' + \gamma_2 x_2' + \omega_2^2 x_2 - \Omega^2 x_1 - \Omega_{c2}^2 x_4 = 0,\\
&x_3'' + \gamma_3 x_3' + \omega_3^2 x_3 - \Omega^2 x_4 - \Omega_c^2 x_1 = \frac{F}{m}\exp(-i\omega_S t),\\
&x_4'' + \gamma_4 x_4' + \omega_4^2 x_4 - \Omega^2 x_3 - \Omega_{c2}^2 x_2 = 0.
\end{aligned} \tag{1}$$

here γ_1, γ_2, γ_3 and γ_4 are the friction constants associated with the energy dissipation, and ω_1, ω_2, ω_3 and ω_4 are oscillation frequencies corresponding to m_1, m_2, m_3, and m_4, respectively. The absorption spectrum can be derived from the solutions of the motion equations (Eq. (1)), and we can fit the absorption spectrum obtained from FDTD simulation (Fig. 2(a)) by using the following set of parameters, i.e., $\omega_1 = \omega_2 = \omega_3 = \omega_4 = 2.86$ eV, $\gamma_1 = \gamma_3 = 2\times10^{-2}$, $\gamma_2 = \gamma_4 = 2.3\times10^{-1}$, $\Omega = 0.78$, $\Omega_c = 0.6$, $\Omega_{c2} = 0.61$.

The time-averaged intensity distributions in the central cross section (*zx* plane) for different wavelengths are illustrated in Fig. 3, which shows that the enhancement of the EM field is more significant at the peak absorption wavelength, e.g. 430 nm, comparing to a non-resonance wavelength, i.e. 532 nm. The resonance intensity at the center of the gap is plotted along the *z* direction (Fig. 4). It is noted that the electric field intensity at wavelength 430 nm

#164468 - $15.00 USD Received 9 Mar 2012; revised 28 Apr 2012; accepted 5 Jun 2012; published 19 Jun 2012

is approximately 2.3 times stronger than the intensity at the non-resonance absorption wavelength of 532 nm.

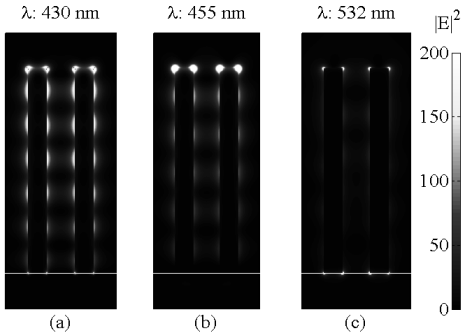

Fig. 3. Intensity distributions of the nanostructure with diameter *d* of 70 nm, height *h* of 820 nm, separation *s* of 100 nm at excitation wavelengths λ of (a) λ: 430 nm, (b) λ: 455 nm and (c) λ: 532 nm, in the *zx* cross section. The white line indicates the interface. Colorbar is in unit of $V^2\ m^{-2}$.

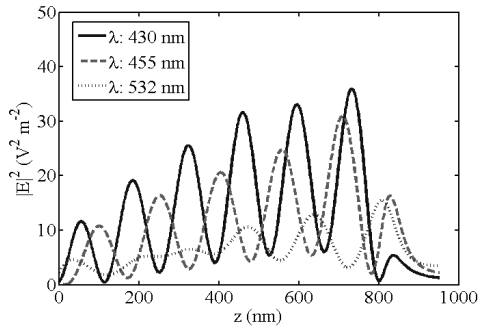

Fig. 4. Comparison of intensity distributions of the nanostructure with diameter *d* of 70 nm, height *h* of 820 nm, separation *s* of 100 nm at different wavelengths at the center of the gap along the *z* direction.

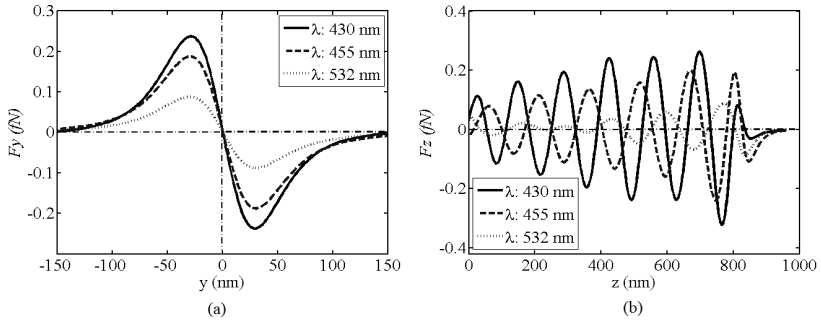

Fig. 5. Comparison of the EM force in the nanostructure with diameter *d* of 70 nm, height *h* of 820 nm, separation *s* of 100 nm at different wavelengths, at the center of the gap. (a) The maximal *Fy*, (b) *Fz*. The intensity of the incident light is taken as 0.1 $mW\cdot\mu m^{-2}$.

To investigate how excitation wavelength affects the trapping of the nanoparticles, the electromagnetic trapping force (EM force) on a 20 nm nanosphere of refractive index of 1.5 is calculated at two peak absorption wavelengths, 430 nm and 455 nm, and one non-peak absorption wavelength 532 nm. The intensity of the excitation is taken as 0.1 $mW\cdot\mu m^{-2}$,

#164468 - $15.00 USD Received 9 Mar 2012; revised 28 Apr 2012; accepted 5 Jun 2012; published 19 Jun 2012

which is about the field intensity illuminating on the nanostructure by a light beam of input power of 10 mW focused by an objective lens of a numerical aperture of 0.5 as used in the previous work [10]. *Fy* is the *y* component of trapping forces along the *y* direction measured in a central cross section of the gap, and *Fz* is the *z* component of trapping forces along the *z* direction measured at the center of the gap. Comparisons of *Fy* and *Fz* of the EM force at peak and non-peak absorption wavelengths are illustrated in Figs. 5(a) and 5(b), respectively. It is shown that the optical trapping efficiencies at the peak absorption wavelength in the *y* and *z* directions are a factor of 2.7 and 3.7 stronger comparing with those at non-resonance wavelength, respectively.

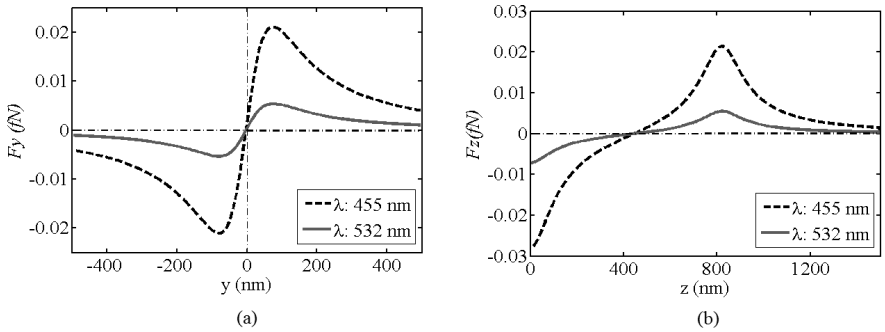

Fig. 6. Comparison of the thermal force in the nanostructure with diameter *d* of 70 nm, height *h* of 820 nm, separation *s* of 100 nm at different wavelengths, at the center of the gap. (a) *Fy*, (b) *Fz*. The intensity of the incident light is taken as 0.1 $mW \cdot \mu m^{-2}$. The Soret coefficient S_T used for calculation is 2 x 10^{-4} (K^{-1}).

One of the major concerns of plasmonic trapping is the considerable heat generated from plasmonic absorption, in which case the thermal force acting on the nanoparticles can be significant [10]. The thermal force acting on the 20 nm nanosphere in a plane 690 nm above the interface is shown in Fig. 6. The Soret coefficient is assumed as $S_T = 2 \times 10^{-4}\ K^{-1}$ according to reported experimental data [27–29]. It should be pointed out that vapor bubbles may form around the plasmonic nanostructure under high laser power excitation [18]. For the plasmonic nanoparticle trapping, bubbles formation can be avoided by controlling the incident power or wavelength. The maximum temperature increase at wavelength of 455 nm is 11 K for incident intensity of 0.1 $mW \cdot \mu m^{-2}$. Under such moderate temperature increase in the surrounding medium [10] and the constant S_T, the thermal force at the peak absorption wavelength (e.g. 455 nm) is approximately five times stronger than that at the non-peak absorption wavelength (e.g. 532 nm) in either the transverse force *Fy* or the axial forces *Fz* due to strong plasmonic absorption. Because the thermal force is far greater than the EM force in the region outside of the nanostructure, the significant increase makes it strong enough to vary transport of nanoparticles [10].

3. Optimization of the nanostructure

3.1 The separation

It is demonstrated in the last section that the plasmonic nano-waveguides structure exhibits significantly stronger enhancement of the resonance field at absorption peaks (e.g. 430 nm or 455 nm). It is expected that the absorption peak is associated with the geometric parameters such as the size (diameter and height) of the rods, and the separation between them. Firstly we fix the size of each rod, i.e. diameter *d*: 70 nm, height *h*: 820 nm, and vary the separation *s*. Figure 7 shows the absorption spectra of the two silver nanorods nanostructures with different separations of 40 nm, 70 nm and 100 nm. It is noted that the absorption peaks are red-shifted while decreasing the separation *s*.

#164468 - $15.00 USD Received 9 Mar 2012; revised 28 Apr 2012; accepted 5 Jun 2012; published 19 Jun 2012

The overall electric field enhancement of the nanostructure is strong at the peak absorption wavelength because of the large dimension of height of the nanorods. In Figs. 8(a-c) the field intensity distributions of the nanostructures with different separations at wavelengths corresponding to the absorption peaks are shown. It is apparent that the field intensity at the gap can be enhanced by decreasing the separation between the two nanorods. The intensity distribution at the center of the gap along the *z* direction is plotted in Fig. 9. It shows that by reducing the separation size from 100 nm to 40 nm, the field intensity at the center the gap is increased almost by one order of magnitude.

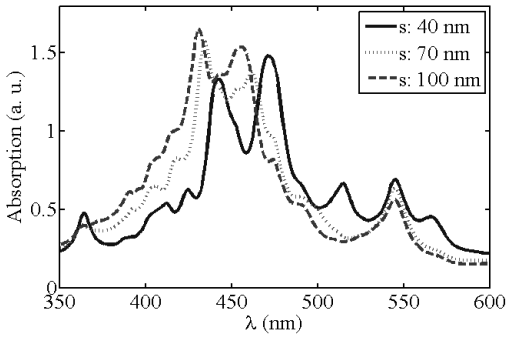

Fig. 7. Absorption spectra of the nanostructure with different separations *s*, for fixed diameter *d* of 70 nm and height *h* of 820 nm.

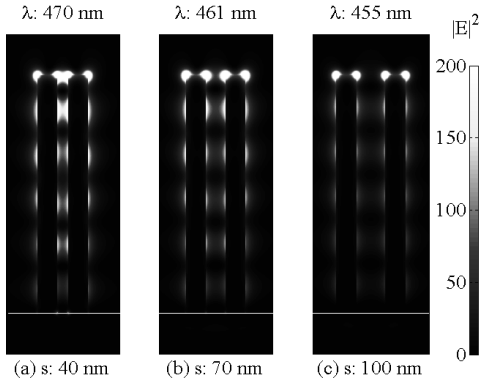

Fig. 8. Intensity distributions in the central cross section (*zx* plane) of the nanostructure with different separations *s* at the corresponding peak absorption wavelengths λ. (a) *s* = 40 nm at λ = 470 nm, (b) *s* = 70 nm at λ = 461 nm, and (c) *s* = 100 nm at λ = 455 nm. Colorbar is in unit of $V^2 m^{-2}$.

The EM force on a 20 nm nanosphere in the central cross section at the gap is show in Fig. 10. While the gap between the two nanorods decreased from 100 nm to 40 nm, *Fy* is enhanced by a factor of 19.5. Similar trend is also found in *Fz*, i.e. the maximal *Fz* increases by a factor of 20, when the separation decreases from 100 nm to 40 nm (Fig. 10(b)). Combining the improvement obtained by tuning towards the resonance wavelength, the EM force can be improved by two orders of magnitude by optimizing the plasmonic nanostructures, comparing with the unoptimised case reported in the previous work [10]. For example, strong EM trapping force as high as 4.7 fN can be obtained with a low incident intensity of 0.1 $mW \cdot \mu m^{-2}$ (Fig. 10(b)). The strength of the EM force is strong enough to trap the nanoparticle considering that trapping a 20 nm nanoparticle requires trapping force larger than approximately 1 fN to overcome the influence of Brownian motion [14, 19, 26]. At the same illumination intensity, the EM force on the 20 nm nanoparticle at the resonance planes can

#164468 - $15.00 USD Received 9 Mar 2012; revised 28 Apr 2012; accepted 5 Jun 2012; published 19 Jun 2012

reach ~2 x 10^{-2} fN for the nanostructure in the previous work. Also the EM force produced by an objective lens (NA = 0.5) at the same illumination strength is approximately 3 x 10^{-4} fN, a total of four orders of magnitude enhancement in trapping force can be achieved with the optimized nanostructure comparing to the case without the nanostructures [10]. In Fig. 11 the thermal force acting on a 20 nm nanosphere is illustrated. With moderate temperature increase in the surrounding medium, e.g. 11 K with incident intensity of 0.1 mW·μm^{-2}, and constant S_T, the thermal force does not show significant variation if the separation changes from 40 nm to 100 nm, despite significant changes in the EM force.

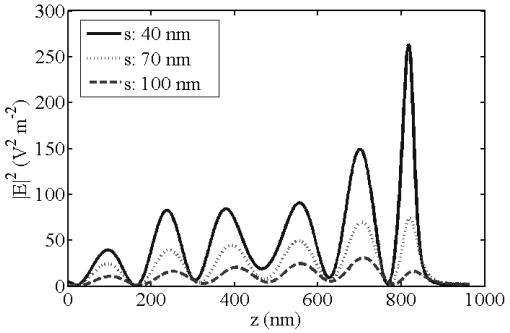

Fig. 9. Comparison of intensity distributions at the center of the gap along the z direction for the nanostructures with different separations s at the corresponding peak absorption wavelengths λ of 470 nm, 461 nm and 455 nm.

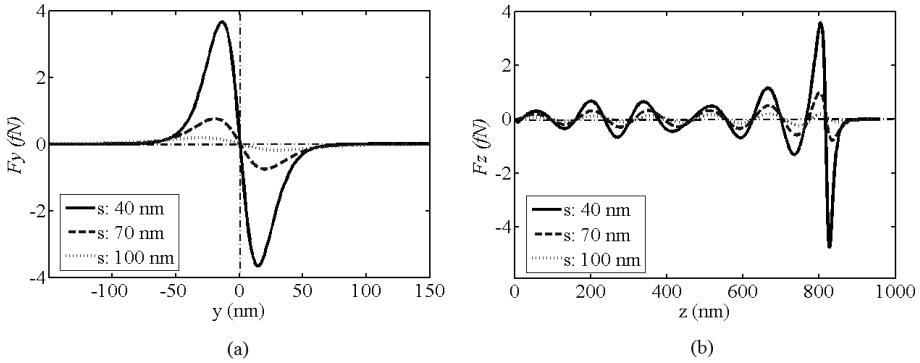

Fig. 10. Comparison of the EM force in the nanostructures with different separations s at the corresponding peak absorption wavelengths λ of 470 nm, 461 nm and 455 nm, respectively. (a) The maximal Fy, (b) Fz. The intensity of the incident light is taken as 0.1 mW·μm^{-2}.

#164468 - $15.00 USD Received 9 Mar 2012; revised 28 Apr 2012; accepted 5 Jun 2012; published 19 Jun 2012

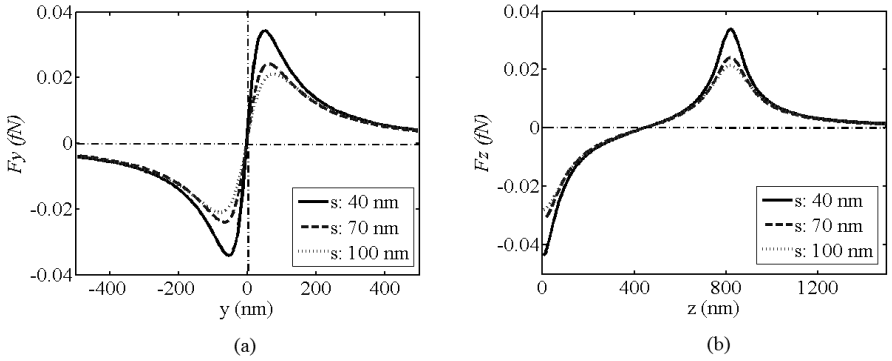

Fig. 11. Comparison of the thermal force in the nanostructure with different separations *s* at the corresponding peak absorption wavelengths λ of 470 nm, 461 nm and 455 nm, respectively: (a) *Fy*, (b) *Fz*. The intensity of the incident light is taken as 0.1 mW·μm^{-2}. The Soret coefficient S_T used for calculation is 2 x 10^{-4} (K^{-1}).

3.2 Effect of the diameter of the nanorod

The absorption spectra of the nanostructure with different diameters of nanorods are shown in Fig. 12. There is a significant shift of peak absorption wavelength (i.e. Δλ: 53 nm) when the diameter of the nanorods changes from 40 nm to 100 nm. It is shown in Fig. 13(a) that the field intensity in the nanostructure with diameter of 40 nm nanorods becomes very weak even at the peak absorption wavelength of 427 nm. For thin nanowires, it is difficult to excite plasmon resonance by the incident light with polarization direction normal to the long axis of the nanorods [23] due to the fact that the radius of the nanorods (20 nm) is close to the skin depth (~14 nm). Under the circumstance, although the absorption is strong, the plasmon resonance is weak.

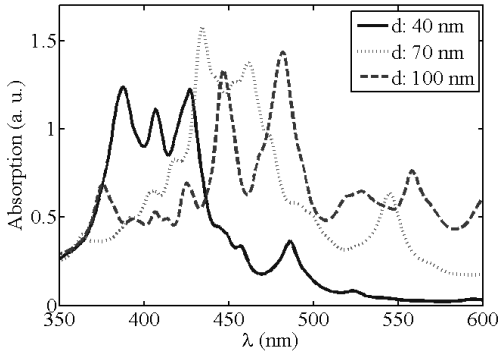

Fig. 12. Absorption spectra of the nanostructure with different diameters *d* at fixed separation *s* of 70 nm and height *h* of 820 nm.

#164468 - $15.00 USD Received 9 Mar 2012; revised 28 Apr 2012; accepted 5 Jun 2012; published 19 Jun 2012

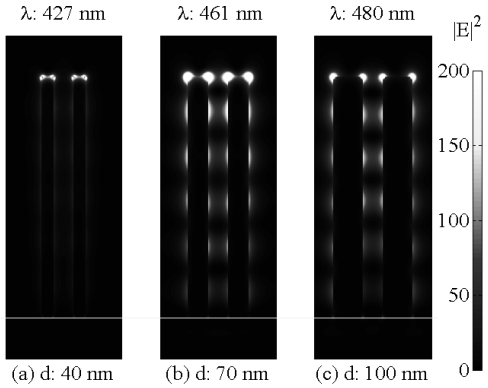

Fig. 13. Intensity distributions of the nanostructure with different diameters d at the corresponding peak absorption wavelengths λ. (a) d = 40 nm at λ = 427 nm, (b) d = 70 nm at λ = 461 nm, and (c) d = 100 nm at λ = 480 nm, in the zx plane. Colorbar is in unit of V^2 m^{-2}.

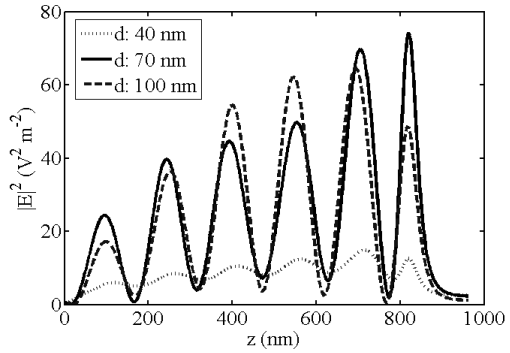

Fig. 14. Comparison of intensity distributions of the nanostructure at the center of the gap along the z direction with different diameters d at the corresponding peak absorption wavelengths λ of 427 nm, 461 nm and 480 nm.

The comparison of the intensity distributions at the center of the gap along the z direction is illustrated in Fig. 14. For the nanorods with diameter larger than 70 nm, the field intensity at the center of the gap does not change noticeably, however accompanied by a peak absorption wavelength shift of 19 nm. Such feature indicates a possible fine tuning capability for plasmon resonance by varying the diameter of the nanorods.

3.3 Effect of the height of the nanorod

The absorption spectra of the nanostructures with different heights of 700 nm, 760 nm and 820 nm are shown in Fig. 15. The diameter of the nanorods and their separation are kept the same (70 nm). It is noticed that the absorption peak wavelength for the same order of plasmon resonance shifts from 461 nm to 437 nm with the height of the nanorods decreased from 820 nm to 700 nm (Fig. 16). The association of plasmon resonance of with the cavity length can be expressed as,

$$\frac{4\pi}{\lambda_{sp}} h = 2m\pi + \varphi. \tag{2}$$

where m is the order of plasmon resonance, λ_{sp} is the plasmon wavelength, φ is the phase shift induced by reflections on the ends of the nanorods [22, 23].

#164468 - $15.00 USD Received 9 Mar 2012; revised 28 Apr 2012; accepted 5 Jun 2012; published 19 Jun 2012

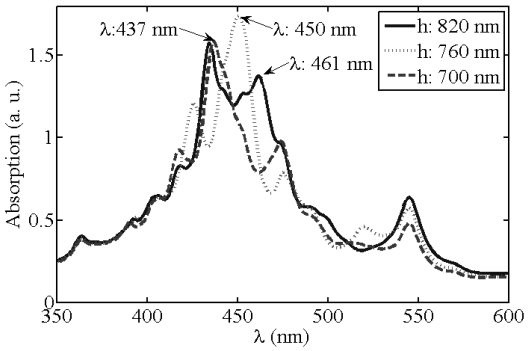

Fig. 15. Absorption spectra of the nanostructure with different heights h of 700 nm, 760 nm and 820 nm, at fixed separation s of 70 nm and diameter d of 70 nm.

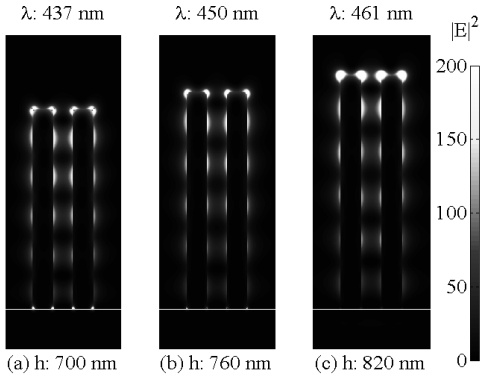

Fig. 16. Intensity distributions of the nanostructure in the zx plane with different heights h at the corresponding peak absorption wavelengths λ. (a) h = 700 nm at λ = 437 nm, (b) h = 760 nm at λ = 450 nm, and (c) h = 820 nm at λ = 461 nm. Colorbar is in unit of V^2 m^{-2}.

The variation of the nanorod length h induces changes in both the plasmon wavelength λ_{sp} and the phase shift φ. The distance between two intensity maxima of the plasmon modes is $\lambda_{sp}/2$, which changes according to the height of the nanorods (Fig. 17(a)). It is also noted that the field intensity around the end of the nanorods exhibits significant variations. This is because that the phase change φ induced by reflections at the ends of nanorods with different heights has a strong effect on the intensity distribution along the nanorods. From Eq. (2), the phase change φ and plasmon wavelength λ_{sp} for nanorods with h = 700 nm, 760 nm, 820 nm, can be obtained as, $\varphi = 0.37\pi$, 0.13π, 0.25π, and λ_{sp} = 270 nm, 300 nm, 320 nm, respectively. When $\varphi = \pi/4$, the field intensity at the end the nanorods (h = 820 nm) is much stronger than the other two cases. As a result, the EM trapping force strength around the end of the nanorods with h = 820 nm, is approximately four times stronger than that of the nanorods with h = 700 nm, as shown in Fig. 17(b). Additionally, the equilibrium trapping positions change with the height of the nanorods under excitations at the peak absorption wavelengths.

#164468 - $15.00 USD Received 9 Mar 2012; revised 28 Apr 2012; accepted 5 Jun 2012; published 19 Jun 2012

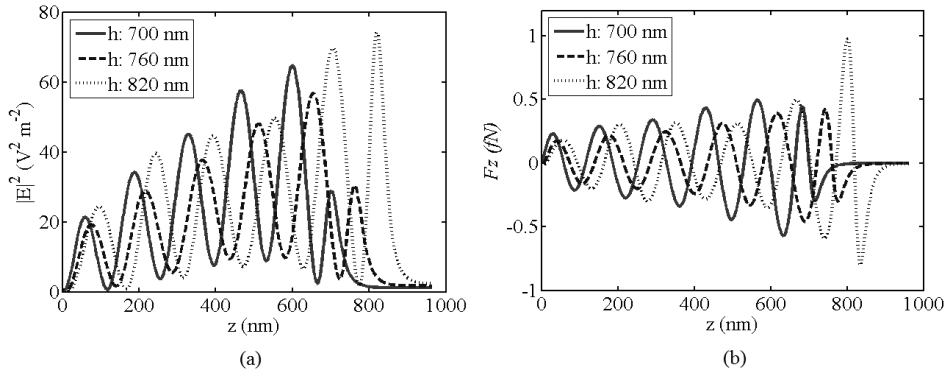

Fig. 17. Comparisons of (a) the intensity distributions, and (b) the EM force, in the nanostructure with different heights h at the center of the gap along the z direction. The corresponding peak absorption wavelengths λ for nanorods of diameter 700 nm, 760 nm and 820 nm are 437 nm, 450 nm and 461 nm, respectively. The intensity of the incident light is taken as 0.1 $mW \cdot \mu m^{-2}$ for force calculation.

4. Discussion

We predict that an improvement of two orders of magnitude in trapping force can be obtained by optimizing the plasmon resonance of the nanostructures. Therefore a total of four orders of magnitude improvement in trapping force can be obtained comparing to the case without the nanostructures [10]. Optical trapping force can be greatly enhanced by tuning the excitation wavelength towards the peak absorption wavelengths of the nanostructure. But such an enhancement in EM force is also accompanied with greater enhancement in the thermally induced forces. As indicated previously [10], the thermal effects are important for plasmonic nanoparticle trapping due to the fact that it has a much wider working range compared to EM force. Reducing the separation between the nanorods can greatly improve the EM trapping force without strongly affecting the thermal force, and this provides us the mechanism to tune the balance between the EM force and the thermal force in order to achieve best nanoparticle trapping performance. The fact that the peak absorption wavelength of the nanostructure is strongly dependent on the diameter of the nanorods offers us the fine tuning capability of the plasmon resonance in practice.

The present results should be of significant importance to attempts to manipulate nanoparticles using plasmonic nanostructures. The high aspect ratio of plasmonic nanostructures is useful for applications such as increasing the packaging density of plasmonic sensors, single molecule assays and nanospectroscopy [5, 9, 16]. Well-defined high aspect ratio plasmonic nanostructures can be fabricated using top-down fabrication processes [7, 33]. The optimization results of this work can be utilized to improve sensing sensitivity and trapping capability using the nanorod plasmonic nanostructures.

#164468 - $15.00 USD Received 9 Mar 2012; revised 28 Apr 2012; accepted 5 Jun 2012; published 19 Jun 2012